International Journal of
Molecular Sciences

MDPI

Article

Experimental and Theoretical Study of N_2 Adsorption on Hydrogenated $Y_2C_4H^-$ and Dehydrogenated $Y_2C_4^-$ Cluster Anions at Room Temperature

Min Gao, Yong-Qi Ding and Jia-Bi Ma *

Key Laboratory of Cluster Science of Ministry of Education, Beijing Key Laboratory of Photoelectronic/Electrophotonic Conversion Materials, School of Chemistry and Chemical Engineering, Beijing Institute of Technology, Beijing 102488, China; 3120201255@bit.edu.cn (M.G.); 3120195628@bit.edu.cn (Y.-Q.D.)
* Correspondence: majiabi@bit.edu.cn

Abstract: The adsorption of atmospheric dinitrogen (N_2) on transition metal sites is an important topic in chemistry, which is regarded as the prerequisite for the activation of robust N≡N bonds in biological and industrial fields. Metal hydride bonds play an important part in the adsorption of N_2, while the role of hydrogen has not been comprehensively studied. Herein, we report the N_2 adsorption on the well-defined $Y_2C_4H_{0,1}^-$ cluster anions under mild conditions by using mass spectrometry and density functional theory calculations. The mass spectrometry results reveal that the reactivity of N_2 adsorption on $Y_2C_4H^-$ is 50 times higher than that on $Y_2C_4^-$ clusters. Further analysis reveals the important role of the H atom: (1) the presence of the H atom modifies the charge distribution of the $Y_2C_4H^-$ anion; (2) the approach of N_2 to $Y_2C_4H^-$ is more favorable kinetically compared to that to $Y_2C_4^-$; and (3) a natural charge analysis shows that two Y atoms and one Y atom are the major electron donors in the $Y_2C_4^-$ and $Y_2C_4H^-$ anion clusters, respectively. This work provides new clues to the rational design of TM-based catalysts by efficiently doping hydrogen atoms to modulate the reactivity towards N_2.

Keywords: N_2 adsorption; mass spectrometry; density functional theory calculations

Citation: Gao, M.; Ding, Y.-Q.; Ma, J.-B. Experimental and Theoretical Study of N_2 Adsorption on Hydrogenated $Y_2C_4H^-$ and Dehydrogenated $Y_2C_4^-$ Cluster Anions at Room Temperature. *Int. J. Mol. Sci.* **2022**, *23*, 6976. https://doi.org/10.3390/ijms23136976

Academic Editor: Reinhard Dallinger

Received: 8 May 2022
Accepted: 20 June 2022
Published: 23 June 2022

1. Introduction

More than 99% of the global nitrogen exists in the shape of gaseous dinitrogen (N_2) in the atmosphere, yet most organisms can only metabolize nitrogen-containing substances such as NH_3 rather than N_2 directly. Although N_2 is the main nitrogen source for most natural and artificial nitrogen-containing compounds, the high bond dissociation energy (9.75 eV) and the large HOMO–LUMO gap (10.8 eV) render its adsorption and activation an enormous challenge in chemistry [1–4]. Scientists regularly rely on transition metal (TM) centers to catalyze the nitrogen conversion processes [5–7]. The initial and critical step in the complicated reduction of dinitrogen is the adsorption of N_2 molecules at the TM center [8,9]. The fixation of nitrogen in industry is carried out at metal-based (Fe^- or Ru^-) catalysts under extremely high temperatures (300–500 °C) and high pressures (100–300 atm), involving the disadvantages of large energy consumption and greenhouse gas emission [10–12]. Thus, it is vital to develop mild, energy-saving, and environment−friendly catalytic systems for N_2 fixation at ambient conditions. The activation of nitrogen by transition metal compounds with the involvement of hydrogen atoms is of particular interest, while the most common feature of N_2 hydrogenative cleavage is the participation of metal hydride bonds [13–15]. A literature survey [13] shows that metal hydride bonds have several important roles: (1) as a hydrogen source; (2) as an electron source for N_2 reduction; (3) as a powerful reducing agent for the removal of activated nitrogen atoms; and so on.

As an ideal model of condensed-phase systems, gas-phase clusters can study chemical reactions and reveal related mechanisms at the strictly molecular level by simulating active sites. [16–19]. Several theoretical and experimental studies have reported the reactivity of metal species with nitrogen, however, only a few metal species such as, Sc_2 [20], Ta_2^+ [21], $V_3C_4^-$ [22], $Ta_2C_4^-$ [23], NbH_2^- [24], $Ta_3N_3H_{0,1}^-$ [25], $Sc_3NH_2^+$ [26], $FeTaC_2^-$ [27], and $AuNbBO^-$ [28] have been characterized to cleave the N≡N triple bond completely. It can be seen that for the studies on N_2 adsorption in the gas phase, there are few metal species, and they mainly focus on the early transition metals. In the previous work, we found that a suitable number of hydrogen atoms has an influence on the reactivity of transition metal-containing clusters with N_2 [24–26,29,30]. $Sc_3NH_2^+$ [26] can effectively realize the activation of N_2 by H_2, which is based on the regulation of N_2 reduction by two H atoms. $Ta_3N_3H_{0.1}^-$ is an example that highlights the importance of the assisted reactivity of a single hydrogen atom, and the reactivity of $Ta_3N_3H^-$ is higher by a factor of five compared with that of $Ta_3N_3^-$ due to the hydrogen atom changing the charge distribution and geometry [25]. How can hydrogen atoms be efficiently doped to modulate the reactivity of TM-containing systems towards N_2 at the molecular scale? Considering the previous exploration of the Sc systems and the fact that Sc and Y belong to the same group, $Y_2C_4^-$ and $Y_2C_4H^-$ cluster anions were synthesized, and the reactivity towards N_2 was investigated by mass spectrometry and DFT calculations, to answer this question. This work clearly revealed that $Y_2C_4H_{0,1}^-$ anions can adsorb N_2, and the hydrogen atom greatly enhances the reactivity of $Y_2C_4H^-$ towards N_2.

2. Results and Discussion

The time-of-flight (TOF) mass spectra of laser ablation-generated, further mass-elected $Y_2C_4^-$ and $Y_2C_4H^-$ cluster anions reacting with N_2 under thermal collision conditions in a linear ion trap (LIT) reactor are shown in Figure 1. The mass spectra for the generation of $Y_2C_4H_{0,1}^-$ clusters has been given (Supplementary Figure S1). Upon the interactions of $Y_2C_4^-$ and $Y_2C_4H^-$ with N_2, two adsorbed complexes that are assigned as $Y_2C_4N_2^-$ and $Y_2C_4HN_2^-$ are observed (Figure 1b,d), suggesting the following channels in Equations (1) and (2):

$$Y_2C_4^- + N_2 \rightarrow Y_2C_4N_2^- \quad (1)$$

$$Y_2C_4H^- + N_2 \rightarrow Y_2C_4HN_2^- \quad (2)$$

Compared with $Y_2C_4^-$, $Y_2C_4H^-$ shows a higher reactivity towards N_2 under the same reaction conditions in Figure 1f. Besides the major products, two weak peaks in Figure 1 are assigned to $Y_2C_4OH^-$ and $Y_2C_4O_2H^-$, generated from the reaction of $Y_2C_4H_{0,1}^-$ anions with water impurities in the LIT. The pseudo-first-order rate constants (k_1) for the reactions one and two are estimated to be $(3.7 \pm 0.8) \times 10^{-12}$ cm^3 molecule^{-1} s^{-1} and $(6.2 \pm 1.3) \times 10^{-14}$ cm^3 molecule^{-1} s^{-1}, which are based on a least-square fitting procedure, corresponding to reaction efficiencies (Φ) [31,32] of 0.6% and 0.01%, respectively. Additionally, the signal dependence of product $Y_2C_4H_{0,1}N_2^-$ ions on N_2 pressures was obtained, which are derived and fitted with the mass spectrometry experimental data (Supplementary Figure S2).

BPW91 calculations are performed to investigate the structures of reactant $Y_2C_4H_{0,1}^-$ anion clusters (Supplementary Figure S3), as well as the reaction mechanisms between $Y_2C_4H_{0,1}^-$ and N_2. The lowest-energy isomer of $Y_2C_4^-$ (doublet, ^{2}**IA1**, Supplementary Figure S3), which is 0.08 eV lower than its quartet isomer, is a C_s-symmetric six−membered ring, with the Y-Y bond as the symmetry axis and two C_2 ligands bonded to the two Y atoms. Moreover, the most stable isomer of $Y_2C_4H^-$ (^{1}**IA2**) has a hydrogen atom binding to the Y1 atom in the six-membered ring, similar to the $Y_2C_4^-$ (^{2}**IA1**), and it is 0.07 eV lower than the triplet state in energy (Supplementary Figure S3). Since the energies of the isomers are very close, their reaction paths are calculated. The results show that, in the reaction coordinates, the energies of the doublet and singlet stationary points and the products in the $Y_2C_4^-/N_2$ and $Y_2C_4H^-/N_2$ systems are lower than those of the corresponding quartet

and triplet analogues, respectively (Supplementary Figure S4). Enthalpy and Gibbs free energies along with electronic and zero-point correction energies are added (Supplementary Table S1). The concentration of dinitrogen adducts in the gas phase is relatively low, so it is difficult to collect and continue to measure Raman spectra. Currently, it is difficult to characterize structures due to technical and instrumental limitations. Infrared multiple photon dissociation may be applied to reveal such types of anions. We have added the calculated infrared spectra (Supplementary Figure S5), and the vibrational frequencies may be used for future experimental identification of these clusters.

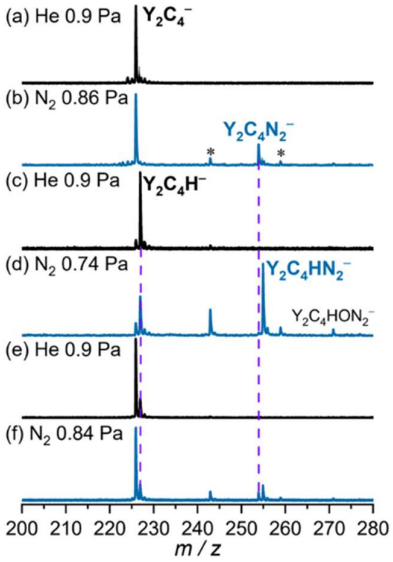

Figure 1. TOF mass spectra for the reactions of (**a**) mass-selected $Y_2C_4^-$ with He and (**b**) N_2 for 6 ms, (**c**) mass-selected $Y_2C_4H^-$ with He and (**d**) N_2 for 14 ms, and (**e**) the coexisting $Y_2C_4^-$ and $Y_2C_4H^-$ clusters with (**f**) N_2 for 10 ms, respectively. The effective reactant gas pressures are shown. The asterisked peaks (*) are $Y_2C_4OH^-$ and $Y_2C_4O_2H^-$, due to the reactions with residual water in the LIT. Black bold, blue bold and black font represent reactants, products and impurities, respectively.

The potential energy surfaces (PESs) of the most favorable reaction pathways are given in Figure 2. The N_2 molecule is initially captured by the Y1 atom in both $Y_2C_4^-$ and $Y_2C_4H^-$ to form the end-on-coordinated complexes ^{2}**I1** and ^{1}**I4**. Notably, ^{2}**I1** (−0.71 eV) in Figure 2a is as stable as ^{1}**I4** (−0.70 eV) in Figure 2b, suggesting that the N_2−adsorbed intermediates ^{2}**I1** and ^{1}**I4** are not the final products in the $Y_2C_4^-/N_2$ and $Y_2C_4H^-/N_2$ systems. As for the $Y_2C_4^-/N_2$ system, the coordination mode of N_2 is further changed from η^1 in ^{2}**I1** to η^2 in ^{2}**I2** via ^{2}**TS1**. During this process, the N-N bond length is elongated from 110 pm in free N_2 to 119 pm in ^{2}**I2**. Subsequently, the adsorbed N_2 unit is anchored by two Y atoms via ^{2}**TS2**, forming a Y-N-N-Y bridge; at the same time, a longer N-N bond of 123 pm is generated in ^{2}**P1**. Note that the rupture of the N-N bonds encounters a high energy barrier (^{2}**TS3**, +2.46 eV with respect to the separated reactants), so that further activation of N_2 is hampered in this system.

The reaction of $Y_2C_4H^-/N_2$ (Figure 2b) follows the similar mechanism. The complex is coordinated laterally to form a Y-N-N-Y bridge like ^{2}**P1** by overcoming a negligible barrier ^{1}**TS4**, and the activation energy (ΔE_a, i.e., the energy difference between the encounter complex and the transition state) is lower than that of ^{2}**I2** → ^{2}**TS2** (ΔE_a = 0.23 eV) in $Y_2C_4^-$. In the step of ^{1}**I4** → ^{1}**P2**, an elongation of the N–N bond from 115 to 121 pm occurs. Further cleavage of N–N is also hindered due to the positive energy barrier of 4.89 eV (^{1}**TS5**). In addition, another adsorption of N_2 on the Y2 atom (Supplementary Figure S6) that is not bonded with the hydrogen atom can be eventually trapped in ^{1}**P2** by generating the η^2-mode intermediate ^{1}**I7**. In conclusion, the reactions of $Y_2C_4H^-$ and $Y_2C_4^-$ with N_2 result in the formation of bridging adsorption products ^{2}**P1** and ^{1}**P2**, and the adsorbed N_2

molecules are in the η^1:η^2 mode. As shown in Figure 3, the potential energy curves reveal that the adsorption process of $Y_2C_4H^-/N_2$ is more favorable kinetically compared to that of $Y_2C_4^-/N_2$, since it is barrier−free for $Y_2C_4H^-/N_2$. A small barrier exists in the shallow entrance channels when N_2 approaches $Y_2C_4^-$, which further explains the experimental observed low reaction rate constant for the dehydrogenated $Y_2C_4^-/N_2$.

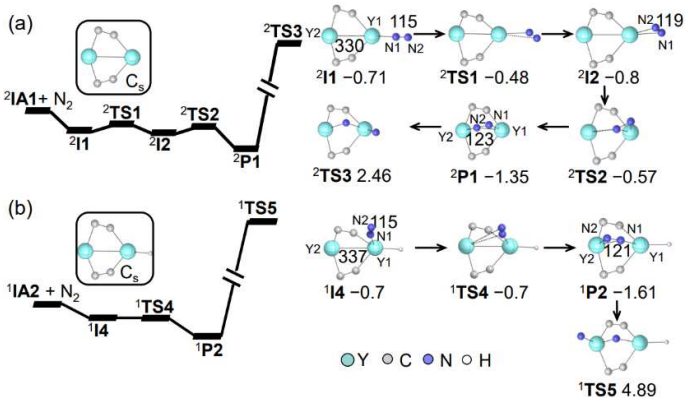

Figure 2. BPW91-D3-calculated potential energy surfaces for the reactions of $Y_2C_4^-$ (**a**) and $Y_2C_4H^-$ (**b**) with N_2. The zero-point vibration-corrected energies (ΔH_{0K} in eV) of the reaction intermediates (**I1**–**I4**), transition states (**TS1**–**TS4**), and products (**P1**, **P2**), with respect to the separated reactants, are given. The bond lengths are given in pm. The green, blue, grey and white atoms represent Y, N, C and H atoms, respectively. Spin multiplicity is located in superscript.

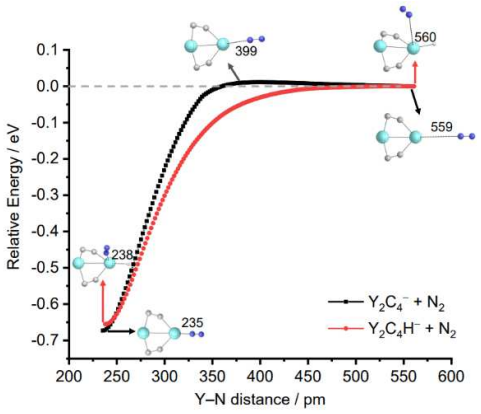

Figure 3. The BPW91-calculated relaxed potential energy curves of N_2 approaching $Y_2C_4^-$ and $Y_2C_4H^-$ anions.

Frontier orbital analysis shows that the immobilization of the N_2 ligand, as well as the formation of ^{2}**P1** and ^{1}**P2**, involve *d*-electrons transfer from the single-occupied molecular orbital-1 (SOMO-1) of $Y_2C_4^-$ and the HOMO orbital of $Y_2C_4H^-$ to the antibonding π^*-orbitals of N_2 (Supplementary Figure S7). The presence of hydrogen atoms enhances the reactivity of the cluster cations toward N_2 since it changes the charge distribution. As shown in Figure 4a, the Y1 linked to the hydrogen atom on the $Y_2C_4H^-$ cluster has more negative charges compared to $Y_2C_4^-$, and it promotes π-back-donation. Note that the energy differences between the transition states and the separated reactants, which is the apparent barrier ($\Delta E^‡$), matters in gas−phase studies. The apparent barrier for $Y_2C_4H^-/N_2$ ($\Delta E^‡ = -0.70$ eV) is lower than that of $Y_2C_4^-/N_2$ ($\Delta E^‡ = -0.48$ eV), and the energy of ^{1}**P2** is lower than that of ^{2}**P1** (−1.61 eV vs. −1.35 eV). According to the Rice-Ramsperger-Kassel-Marcus (RRKM) theory [33], the internal conversion rate of **I4** → **TS4** (8.49×10^{11} s^{-1}) is 32 times larger than that of **I2** → **TS2** (2.65×10^{10} s^{-1}). These theoretical results are consistent with the experiments.

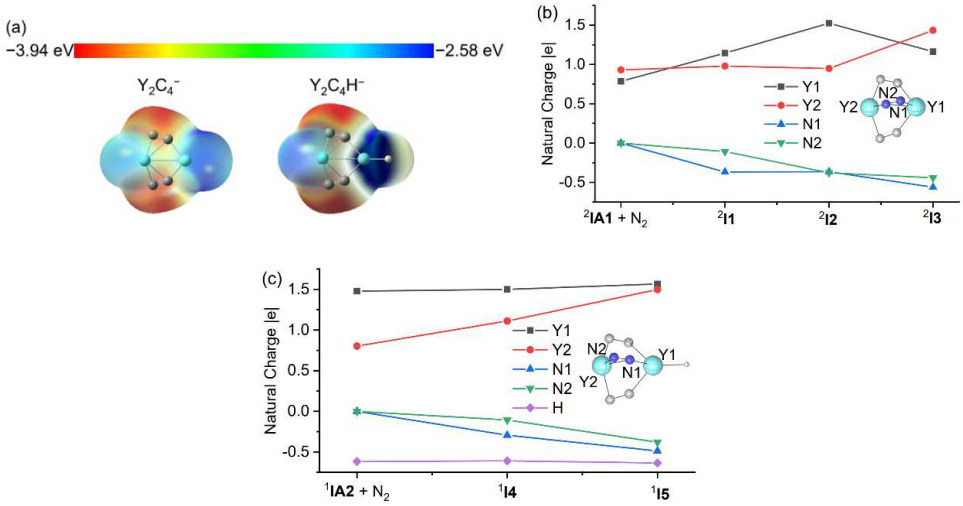

Figure 4. (**a**) Electrostatic potentials of the $Y_2C_4H_{0,1}^-$. Charges on atoms of stationary points along reaction coordinates of N_2 absorption on (**b**) $Y_2C_4^-$ and (**c**) $Y_2C_4H^-$ clusters.

To further improve the understanding of $Y_2C_4H_{0,1}^-/N_2$ systems, NBO analysis along reaction coordinates was performed (Figure 4b,c). The charge details were added (Supplementary Table S2). In the adsorption processes **IA1** → **I1** and **IA2** → **I4** of $Y_2C_4H_{0,1}^-/N_2$, the yttrium atoms transfer 0.37 *e* and 0.29 *e* to the N1 atom, respectively, leading to the formation of the Y-N1 bonds, while two N2 atoms in Y2C4$^-$ and $Y_2C_4H^-$ only increase by 0.11 *e*. In the subsequent steps **I2** → **P1** and **I4** → **P2** for the formation of the N2-Y2 bonds, more electrons are stored in the two nitrogen atoms, resulting in the gradual elongation of the N-N bonds. Overall, the electrons required for the N_2 adsorption by the $Y_2C_4^-$ and $Y_2C_4H^-$ clusters are mainly provided by Y atoms with total transferred amounts of 0.88 *e* and 0.78 *e*, respectively. Differently, two and one Y atoms are the electron donors in $Y_2C_4^-$ and $Y_2C_4H^-$, respectively. The active Y1 atom in $Y_2C_4^-$ (**IA1**) has more 5s electron occupancies ($5s^{1.10}$ $4d^{1.03}$), which causes an unfavorable approach and a high σ-repulsion on the N_2 molecule. When one hydrogen atom on the $Y_2C_4^-$ (^{2}**IA1**) cluster bonds to form $Y_2C_4H^-$ (^{1}**IA2**), the natural charge on the Y1 increases from 0.79 *e* to 1.48 *e*; at the same time, more 4*d* and less 5*s* electron occupancies are located ($5s^{0.38}$ $4d^{1.12}$), which can make N_2 more accessible to the $Y_2C_4H^-$ cluster anions. The values of bond orders of Y-Y bond in $Y_2C_4H_{0,1}^-$ anions are an important indicator for the ability of storing electrons, which increases from 0.55 in $Y_2C_4^-$ (^{2}**IA1**) to 0.66 in $Y_2C_4H^-$ (^{1}**IA2**). Therefore, although hydrogen appears to be a bystander in N_2 adsorption, its presence indeed stores more electrons in the Y-Y bond and facilitates N_2 adsorption. It can be concluded that the hydrogen atom in the $Y_2C_4H^-$ cluster significantly affects the charge distribution and electronic structure, and a suitable number of hydrogen atoms can enhance the reactivity towards N_2.

3. Methods

3.1. Experimental Methods

The metal carbide clusters were generated by laser ablation metal target (made of pure yttrium powder) (Jiangxi Ketai New Materials Co. Ltd, Jiangxi, China) seeded at 2‰ CH_4(Beijing Huatong Jingke Gas Chemical Co. Ltd, Beijing, China) in a helium carrier gas (backing pressure 4 atm). The pulsed laser is a 532 nm laser with 5–8 mJ/energy pulses and 10 Hz repetition rate (140 Baytech Drive, San Jose, CA, USA). $Y_2C_4^-$ and $Y_2C_4H^-$ anion clusters were mass-selected by a quadrupole mass filter (QMF) (China Academy of Engineering Physics, Mianyang, Sichuan, China) [34] and subsequently entered into a linear ion trap (LIT) reactor (homemade) [35]. After being confined and thermalized by the pulsed gas He for about 2 ms, they interacted with N_2 for about 6 ms and 14 ms, at room temperature, respectively. The anion clusters were ejected from the LIT and then detected by a reflection time-of-flight mass spectrometer (TOF-MS) [36]. The rate constants

of the reactions between $Y_2C_4H_{0,1}^-$ cluster anions and N_2 were described [37]. A schematic diagram of the experimental apparatus is shown in ref [34].

3.2. Computational Methods

All DFT [38] calculations were formed using the Gaussian 09 [39] program package to explore the structures of reactant clusters $Y_2C_4H_{0,1}^-$ and the mechanistic details of $Y_2C_4H_{0,1}^-$ with N_2. To give the best interpretation of the experimental data, we calculated the dissociation energies of the Y-Y Y-C, N-N and C-C (Supplementary Table S3) bonds using 20 methods. The results show that BPW91 functional [40–42] performs very well. For application of basis sets in reaction systems, the def2-TZVP [43] basis set was used for the Y atom, and the 6 − 311 + G * basis sets [44,45] were selected for the C, H, and N atoms, which were applied in other systems containing these elements [24,27,46]. The zero-point vibration corrected energies (ΔH_{0K} in eV) in unit of eV are reported. Vibrational frequency calculations must be performed for the geometric optimization of the reaction intermediates (**I**Ms) and transition states (**TS**s) [47]. Intrinsic reaction coordinate [48] calculations were employed to ensure whether each TS was connected to two appropriate local minima. DFT-D3 correction for the complexes were contained in the system. Natural population analysis was performed using NBO 6.0 [49], and the orbital composition was analyzed by the method of natural atomic orbitals employing the Multiwfn program [50].

4. Conclusions

In summary, the reactions of $Y_2C_4H^-$ and dehydrogenated $Y_2C_4^-$ cluster anions with N_2 have been investigated experimentally and theoretically. The experimental results indicate that the reaction rate constant of $Y_2C_4H^-/N_2$ is higher by a factor of 50 compared with that of $Y_2C_4^-/N_2$. DFT calculations indicate that the differences are caused by the different charge distributions and the bonding of the additional hydrogen atom to the yttrium atom in the $Y_2C_4H^-$ cluster, resulting in more 4d electron occupancies and thus more efficient π-back-donation bonding with N_2 molecules. The electron donor atoms of $Y_2C_4^-$ and $Y_2C_4H^-$ anion clusters are different, for $Y_2C_4^-$, two Y atoms donate electrons, while only one Y atom donates electrons in $Y_2C_4H^-$. Storing more electrons in the Y-Y bond is also an important influence of the hydrogen atom on the reactivity of $Y_2C_4H^-$ to N_2. This study clearly reveals the significance of hydrogen-assisted reactions in N_2 adsorption processes. Attaching an appropriate number of hydrogen atoms on active sites can enhance the N_2 adsorption rates, providing a new strategic direction for the rational design of TM-based energy-efficient nitrogen fixation catalysts.

Supplementary Materials: The following supporting information can be downloaded at: https://www.mdpi.com/article/10.3390/ijms23136976/s1. References [51–55] are cited in the supplementary materials.

Author Contributions: Data curation, M.G. and Y.-Q.D.; writing—original draft preparation, M.G.; writing—review and editing, M.G. and J.-B.M.; supervision, J.-B.M.; project administration, J.-B.M.; funding acquisition, J.-B.M. All authors have read and agreed to the published version of the manuscript.

Funding: This research was funded by National Natural Science Foundation of China (No. 91961122) and the Beijing Natural Science Foundation (No. 2222023).

Institutional Review Board Statement: Not applicable.

Informed Consent Statement: Not applicable.

Data Availability Statement: The data presented in this study are available on request from the corresponding author.

Conflicts of Interest: The authors declare no conflict of interest.

References

1. Burford, R.J.; Fryzuk, M.D. Examining the relationship between coordination mode and reactivity of dinitrogen. *Nat. Rev. Chem.* **2017**, *1*, 0026. [CrossRef]
2. Chen, J.G.; Crooks, R.M.; Seefeldt, L.C.; Bren, K.L.; Bullock, R.M.; Darensbourg, M.Y.; Holland, P.L.; Hoffman, B.; Janik, M.J.; Jones, A.K.; et al. Beyond fossil fuel–driven nitrogen transformations. *Science* **2018**, *360*, eaar6611. [CrossRef] [PubMed]
3. Légaré, A.; Rang, M.; Bélanger-Chabot, G.; Schweizer, J.I.; Krummenacher, I.; Bertermann, R.; Arrowsmith, M.; Holthausen, M.C.; Braunschweig, H. The reductive coupling of dinitrogen. *Science* **2019**, *363*, 1329–1332. [CrossRef] [PubMed]
4. Tomaszewski, R. Citations to chemical resources in scholarly articles: CRC handbook of chemistry and physics and the merck index. *Scientometrics* **2017**, *112*, 1865–1879. [CrossRef]
5. Avenier, P.; Taoufik, M.; Lesage, A.; Solans-Monfort, X.; Baudouin, A.; de Mallmann, A.; Veyre, L.; Basset, J.M.; Eisenstein, O.; Emsley, L.; et al. Dinitrogen dissociation on an isolated surface tantalum atom. *Science* **2007**, *317*, 1056–1060. [CrossRef]
6. Shima, T.; Hu, S.; Luo, G.; Kang, X.; Luo, Y.; Hou, Z. Dinitrogen cleavage and hydrogenation by a trinuclear titanium polyhydride complex. *Science* **2013**, *340*, 1549–1552. [CrossRef]
7. Qiu, P.Y.; Wang, J.W.; Liang, Z.Q.; Xue, Y.J.; Zhou, Y.L.; Zhang, X.L.; Cui, H.Z.; Cheng, G.Q.; Tian, J. The metallic 1T-WS2 as cocatalysts for promoting photocatalytic N2 fixation performance of Bi5O7Br nanosheets. *Chin. Chem. Lett.* **2021**, *32*, 3501–3504. [CrossRef]
8. Deng, G.; Pan, S.; Wang, G.; Zhao, L.; Zhou, M.; Frenking, G. Beryllium atom mediated dinitrogen activation via coupling with carbon monoxide. *Angew. Chem. Int. Ed.* **2020**, *59*, 18201–18207. [CrossRef]
9. Wang, Y.Y.; Ding, X.L.; Israel Gurti, J.; Chen, Y.; Li, W.; Wang, X.; Wang, W.J.; Deng, J.J. Non-dissociative activation of chemisorbed dinitrogen on one or two vanadium atoms supported by a Mo_6S_8 cluster. *Chem. Phys. Chem.* **2021**, *22*, 1645–1654. [CrossRef]
10. Qing, G.; Ghazfar, R.; Jackowski, S.T.; Habibzadeh, F.; Ashtiani, M.M.; Chen, C.P.; Smith, M.R., III; Hamann, T.W. Recent advances and challenges of electrocatalytic N_2 reduction to ammonia. *Chem. Rev.* **2020**, *120*, 5437–5516. [CrossRef]
11. Cherkasov, N.; Ibhadon, A.O.; Fitzpatrick, P. A review of the existing and alternative methods for greener nitrogen fixation. *Chem. Eng. Process.* **2015**, *90*, 24–33. [CrossRef]
12. van der Ham, C.J.M.; Koper, M.T.M.; Hetterscheid, D.G.H. Challenges in reduction of dinitrogen by proton and electron transfer. *Chem. Soc. Rev.* **2014**, *43*, 5183–5191. [CrossRef] [PubMed]
13. Jia, H.P.; Quadrelli, E.A. Mechanistic aspects of dinitrogen cleavage and hydrogenation to produce ammonia in catalysis and organometallic chemistry: Relevance of metal hydride bonds and dihydrogen. *Chem. Soc. Rev.* **2014**, *43*, 547–564. [CrossRef] [PubMed]
14. Li, J.; Li, S. Energetics and mechanism of dinitrogen cleavage at a mononuclear surface tantalum center: A new way of dinitrogen reduction. *Angew. Chem. Int. Ed.* **2008**, *47*, 8040–8043. [CrossRef]
15. Chow, C.; Taoufik, M.; Quadrelli, E.A. Cheminform abstract: Ammonia and dinitrogen activation by surface organometallic chemistry on silica-grafted tantalum hydrides. *Eur. J. Inorg. Chem.* **2011**, *2011*, 1349–1359. [CrossRef]
16. Lang, S.M.; Bernhardt, T.M. Gas phase metal cluster model systems for heterogeneous catalysis. *Phys. Chem. Chem. Phys.* **2012**, *14*, 9255–9269. [CrossRef]
17. O'Hair, R.A.J.; Khairallah, G.N. Gas phase ion chemistry of transition metal clusters: Production, reactivity, and catalysis. *J. Clust. Sci.* **2004**, *15*, 331–363. [CrossRef]
18. Schwarz, H. Menage-a-Trois: Single-atom catalysis, mass spectrometry, and computational chemistry. *Catal. Sci. Technol.* **2017**, *7*, 4302–4314. [CrossRef]
19. Schwarz, H. How and why do cluster size, charge state, and ligands affect the course of metal-mediated gas-phase activation of methane? *Isr. J. Chem.* **2014**, *54*, 1413–1431. [CrossRef]
20. Gong, Y.; Zhao, Y.Y.; Zhou, M.F. Formation and characterization of the tetranuclear scandium nitride: Sc_4N_4. *J. Phys. Chem. A* **2007**, *111*, 6204–6207. [CrossRef]
21. Geng, C.; Li, J.L.; Weiske, T.; Schwarz, H. Ta^{2+}-Mediated ammonia synthesis from N_2 and H_2 at ambient temperature. *Proc. Natl. Acad. Sci. USA* **2018**, *115*, 11680–11687. [CrossRef] [PubMed]
22. Li, Z.Y.; Li, Y.; Mou, L.H.; Chen, J.J.; Liu, Q.Y.; He, S.G.; Chen, H. A facile N≡N bond cleavage by the trinuclear metal center in vanadium carbide cluster anions $V_3C_4^-$. *J. Am. Chem. Soc.* **2020**, *142*, 10747–10754. [CrossRef] [PubMed]
23. Li, Z.Y.; Mou, L.H.; Wei, G.P.; Ren, Y.; Zhang, M.Q.; Liu, Q.Y.; He, S.G. C–N coupling in N_2 fixation by the ditantalum carbide cluster anions $Ta_2C_4^-$. *Inorg. Chem.* **2019**, *58*, 4701–4705. [CrossRef] [PubMed]
24. Wang, M.; Chu, L.Y.; Li, Z.Y.; Messinis, A.M.; Ding, Y.Q.; Hu, L.R.; Ma, J.B. Dinitrogen and carbon dioxide activation to form C–N bonds at room temperature: A new mechanism revealed by experimental and theoretical studies. *J. Phys. Chem. Lett.* **2021**, *12*, 3490–3496. [CrossRef]
25. Zhao, Y.; Cui, J.T.; Wang, M.; Valdivielso, D.Y.; Fielicke, A.; Hu, L.R.; Ma, J.B. Dinitrogen fixation and reduction by $Ta_3N_3H_{0,1}^-$ cluster anions at room temperature: Hydrogen-assisted enhancement of reactivity. *J. Am. Chem. Soc.* **2019**, *141*, 12592–12600. [CrossRef]
26. Wang, M.; Zhao, C.Y.; Zhou, H.Y.; Zhao, Y.; Li, Y.K.; Ma, J.B. The sequential activation of H_2 and N_2 mediated by the gas-phase Sc3N+ clusters: Formation of amido unit. *J. Chem. Phys.* **2021**, *154*, 054307. [CrossRef]
27. Mou, L.H.; Li, Y.; Li, Z.Y.; Liu, Q.Y.; Chen, H.; He, S.G. Dinitrogen activation by heteronuclear metal carbide cluster anions $FeTaC_2^-$: A 5d early and 3d late transition metal strategy. *J. Am. Chem. Soc.* **2021**, *143*, 19224–19234. [CrossRef]

28. Li, Y.; Ding, Y.Q.; Zhou, S.D.; Ma, J.B. Dinitrogen activation by dihydrogen and quaternary cluster anions AuNbBO$^-$: Nb− and B−Mediated N_2 activation and Au-assisted nitrogen transfer. *J. Phys. Chem. Lett.* **2022**, *13*, 4058–4063. [CrossRef]
29. Mou, L.H.; Li, Z.Y.; Liu, Q.Y.; He, S.G. Size-dependent association of cobalt deuteride cluster anions $Co_3D_n^-$ (n = 0–4) with dinitrogen. *J. Am. Soc. Mass Spectrom.* **2019**, *30*, 1956. [CrossRef]
30. Cheng, X.; Li, Z.Y.; Mou, L.H. Size-dependent reactivity of rhodium deuteride cluster anions $Rh_3D_n^-$ (n = 0–3) toward dinitrogen: The prominent role of σ donation. *J. Chem. Phys.* **2022**, *156*, 064303. [CrossRef]
31. Gioumousis, G.; Stevenson, D.P. Reactions of gaseous molecule ions with gaseous molecules. *J. Chem. Phys.* **1958**, *29*, 294–299. [CrossRef]
32. Kummerlöwe, G.; Beyer, M.K. Rate estimates for collisions of ionic clusters with neutral reactant molecules. *Int. J. Mass Spectrom.* **2005**, *244*, 84–90. [CrossRef]
33. Steinfeld, J.I.; Francisco, J.S.; Hase, W.L. *Chemical Kinetics and Dynamics*; Prentice-Hall: Hobboken, NJ, USA, 1999; p. 231.
34. Yuan, Z.; Zhao, Y.X.; Li, X.N.; He, S.G. Reactions of $V_4O_{10}^+$ cluster ions with simple inorganic and organic molecules. *Int. J. Mass Spectrom.* **2013**, *354–355*, 105–112. [CrossRef]
35. Jiang, L.X.; Liu, Q.Y.; Li, X.N.; He, S.G. Design and application of a high-temperature linear ion trap reactor. *J. Am. Soc. Mass Spectrom.* **2018**, *29*, 78–84. [CrossRef]
36. Wu, X.N.; Xu, B.; Meng, J.H.; He, S.G. C−H bond activation by nanosized scandium oxide clusters in gas-phase. *Int. J. Mass Spectrom.* **2012**, *310*, 57–64. [CrossRef]
37. Li, Z.Y.; Yuan, Z.; Li, X.N.; Zhao, Y.X.; He, S.G. CO oxidation catalyzed by single gold atoms supported on aluminum oxide clusters. *J. Am. Chem. Soc.* **2014**, *136*, 14307–14313. [CrossRef]
38. Chan, B.; Gill, P.M.W.; Kimura, M. Assessment of DFT methods for transition metals with the TMC151 compilation of data sets and comparison with accuracies for main group chemistry. *J. Chem. Theory. Comput.* **2019**, *15*, 3610–3622. [CrossRef]
39. Frisch, M.J.; Trucks, G.W.; Schlegel, H.B.; Scuseria, G.E.; Robb, M.A.; Cheeseman, J.R.; Scalmani, G.; Barone, V.; Mennucci, B.; Petersson, G.A.; et al. *Gaussian 09, revision A.1*; Gaussian, Inc.: Wallingford, CT, USA, 2009.
40. Lee, C.T.; Yang, W.T.; Parr, R.G. Development of the collesalvetti correlation-energy formula into a functional of the electrondensity. *Phys. Rev. B* **1988**, *37*, 785–789. [CrossRef]
41. Becke, A.D. Density-functional exchange-energy approximation with correct asymptotic-behavior. *Phys. Rev. A* **1988**, *38*, 3098–3100. [CrossRef]
42. Becke, A.D. Density-functional Thermochemistry III. The role of exact exchange. *J. Chem. Phys.* **1993**, *98*, 5648–5652. [CrossRef]
43. Gonzalez, C.; Schlegel, H.B. Reaction path following in mass-weighted internal coordinates. *J. Chem. Phys.* **1990**, *94*, 5523–5527. [CrossRef]
44. Krishnan, R.; Binkley, J.S.; Seeger, R.; Pople, J.A. Self-consistent molecular-orbital methods 0.20. basis set for correlated wave-functions. *J. Chem. Phys.* **1980**, *72*, 650–654. [CrossRef]
45. Clark, T.; Chandrasekhar, J.; Spitznagel, G.W.; Schleyer, P.V.R. Efficient diffuse function-augmented basis sets for anion calculations. III.* The 3-21+G Basis set for first-row elements, Li-F. *J. Comput. Chem.* **1983**, *4*, 294–301. [CrossRef]
46. Ma, J.B.; Wang, Z.C.; Schlangen, M.; He, S.G.; Schwarz, H. On the Origin of the Surprisingly Sluggish Redox Reaction of the N_2O/CO Couple Mediated by $[Y_2O_2]^{+\bullet}$ and $[YAlO_2]^{+\bullet}$ Cluster Ions in the Gas Phase. *Angew. Chem. Int. Ed.* **2013**, *52*, 1226–1230. [CrossRef] [PubMed]
47. Berente, I.; Náray-Szabó, G. Multicoordinate driven method for approximating enzymatic reaction paths: Automatic definition of the reaction coordinate using a subset of chemical coordinates. *J. Phys. Chem. A.* **2006**, *110*, 772–778. [CrossRef] [PubMed]
48. Gonzalez, C.; Schlegel, H.B. An improved algorithm for reaction path following. *J. Chem. Phys.* **1989**, *90*, 2154–2161. [CrossRef]
49. Glendening, E.D.; Badenhoop, J.K.; Reed, A.E.; Carpenter, J.E.; Bohmann, J.A.; Morales, C.M.; Landis, C.R.; Weinhold, F. *NBO 6.0*; Theoretical Chemistry Institute, University of Wisconsin: Madison, WI, USA, 2013. Available online: http://nbo6.chem.wisc.edu/ (accessed on 20 January 2022).
50. Lu, T.; Chen, F.W. Multiwfn: A multifunctional wavefunction analyzer. *J. Comput. Chem.* **2012**, *33*, 580–592. [CrossRef]
51. Beyer, T.; Swinehart, D.F. Algorithm 448: Number of Multiply-Restricted Partitions. *Commun. ACM* **1973**, *16*, 379. [CrossRef]
52. Simoes, J.A.M.; Beauchamp, J.L. Transition metal-hydrogen and metal-carbon bond strengths: The keys to catalysis. *Chem. Rev.* **1990**, *90*, 629–688. [CrossRef]
53. Mallard, W.G. (Ed.) *NIST Chemistry Webbook*; August 1990. Available online: http://webbook.nist.gov (accessed on 20 January 2022).
54. Gurvich, L.V.; Karachevtsev, G.V. *Bond Energies of Chemical Bonds, Ionization Potentials and Electron Affinities*; Nauka: Moscow, Russia, 1974.
55. Tang, X.N.; Hou, Y.; Ng, C.Y.; Ruscic, B. Pulsed field-ionization photoelectronphotoion coincidence study of the process $N_2 + h\nu \rightarrow N^+ + N + e^-$: Bond dissociation energies of N_2 and N_2^+. *J. Chem. Phys.* **2011**, *123*, 074330. [CrossRef]